

RSC Advances



This is an *Accepted Manuscript*, which has been through the Royal Society of Chemistry peer review process and has been accepted for publication.

Accepted Manuscripts are published online shortly after acceptance, before technical editing, formatting and proof reading. Using this free service, authors can make their results available to the community, in citable form, before we publish the edited article. This *Accepted Manuscript* will be replaced by the edited, formatted and paginated article as soon as this is available.

You can find more information about *Accepted Manuscripts* in the [Information for Authors](#).

Please note that technical editing may introduce minor changes to the text and/or graphics, which may alter content. The journal's standard [Terms & Conditions](#) and the [Ethical guidelines](#) still apply. In no event shall the Royal Society of Chemistry be held responsible for any errors or omissions in this *Accepted Manuscript* or any consequences arising from the use of any information it contains.



Journal Name

ARTICLE

Influence of magnetic fields on the morphology and pseudocapacitive properties of NiO on nickel foam

Yisheng Lu,^a Tao Zhu,^a Guoxiong Zhang,^a Zhenni He,^a Chuan Lin,^b Yigang Chen,^{a,*} Haibo Guo^a

Received 00th January 20xx,
Accepted 00th January 20xx

DOI: 10.1039/x0xx00000x

www.rsc.org/

Nanostructured nickel oxide (NiO) films have been successfully deposited on nickel foam by a simple magnetic-field-assisted hydrothermal method, followed by calcination in air. The NiO thin films consisted of uniformly hexagonal nanoplates when magnetic fields (0–12.6 mT) were applied through an electromagnetic coil. The magnetic field affected the size and growth direction of NiO nanoplates, as well as the electrochemical performance of the NiO nanomaterial. The magnetic-field-assisted NiO electrodes showed better electrochemical performance than NiO electrode synthesized without a magnetic field. The optimal NiO electrode had a specific capacitance of 932.1 F g⁻¹ at 0.5 A g⁻¹, with a retention ratio of 91.9% at 2.0 A g⁻¹ over 1000 cycles. These results indicated that the magnetic-field-assisted method in hydrothermal synthesis of NiO electrodes could be an economical and effective way for high-performance supercapacitors.

Introduction

With depleting fossil fuels and increasing environmental problems, high-performance energy conversion and storage systems, such as supercapacitors, Li-ion batteries, fuel cells, and dye sensitized solar cells, are playing an important role in human society.^{1–3} Among various advanced devices for energy storage, supercapacitors have attracted special attention because of their long cycle life (up to 10⁵–10⁶ cycles), excellent safety, fast charge/discharge rates (within several seconds) and high power density (>10 kW kg⁻¹), making them very promising for applications in hybrid vehicles, consumer electronics, medical electronics, and rechargeable energy systems.^{4,6} Despite their excellent performance, supercapacitors generally cannot be used as stand-alone units for their limited energy density (less than 10 Wh kg⁻¹), and there still remain challenges to make high-performance supercapacitors in a convenient and efficient way. Thus, great efforts are being made to improve the energy density of supercapacitors, while maintaining a high power density, and to develop a facile and general route for producing supercapacitor electrodes.^{5, 7, 8}

Supercapacitors are classified into electric double-layer capacitors (EDLCs) and pseudocapacitors according to the nature of their charge-storage processes. EDLCs host non-faradic reactions involving electrostatic charge diffusion and accumulation at interfaces of electrode/electrolyte, whereas pseudocapacitors involve Faradic processes, i.e., fast surface redox reactions.^{9, 10} Generally, pseudocapacitors deliver 3–4 times higher capacitance than EDLCs because the Faradic redox reaction happens not only on the surface, but also at places near the surface of the active

electrode.³ Hydrated RuO₂ is one of the most efficient electrode materials and has been widely studied due to its high pseudocapacitance, reversible charge-discharge features, and good electrical conductivity, whereas its high cost, toxicity, and the presence of corrosive electrolytes may restrict its commercialization.^{11, 12} As a result, many efforts have been made to replace RuO₂ with other inexpensive transition metal oxides, such as MnO₂,^{13–15} NiO,¹⁶ V₂O₅,¹⁷ and Co₃O₄,¹⁸ as electrode materials.

Among them, NiO has attracted great interests owing to its low cost, natural abundance, and high theoretical specific capacity (2583 F g⁻¹ in a potential window of 0.5 V).^{19–21} However, the intrinsic high resistance (the electrical conductivity is less than 10⁻¹³ Ω⁻¹ cm⁻¹ at room temperature), low specific surface area, and slow ion transport rate of NiO limit its charge-discharge capability and power performance for high-power applications.^{3, 9, 22} To solve these problems, many researchers have synthesized NiO films on conducting substrates (typically nickel foams) to make binder-free and conductive-additive-free electrodes.^{23, 24} For instance, Yan et al.²⁵ investigated the NiO nanosheets deposited on nickel foams by a hydrothermal approach with a post-annealing treatment, and the specific capacitance value was 943.5 F g⁻¹ in 3 M KOH electrolyte. Yang et al.²⁶ fabricated porous NiO nanosheets on nickel foams through a one-step in-situ anodization. A binder-free NiO electrode was reported to have an ultrahigh capacitance (4.74 F cm⁻² at 4 mA cm⁻²), excellent rate capability, and cycling stability. An et al.¹⁹ reported mesoporous NiO nanosheets on nickel foam synthesized by a hydrothermal method, and the as-prepared NiO electrode showed a specific capacitance of 1349 F g⁻¹. From the above reports, it can be seen that direct growth of NiO on nickel foams has such advantages that the morphology of the NiO is controllable, and the electrochemical studies on NiO abound for simple manufacturing processes required for making electrodes.

^a Department of Electronic Information Materials, School of Materials Science and Engineering, Shanghai University, Shanghai 200444, China.

^b China Technology Center, GE Global Research, Shanghai 201203, China.

As both morphology and microstructure play essential roles in the performance of electrode materials, researchers optimize the morphology and microstructure of NiO to improve pseudocapacitive properties by adjusting various reaction parameters, such as temperature, pressure, nickel sources, etc. Magnetic fields, similar to those conventional reaction conditions, have been introduced as an effective tool to control morphology and microstructure of NiO. Several studies have been dedicated to understand how a magnetic field influences the structure and the morphology of nanostructured NiO^{27, 2827, 28}. However, little work has aimed to understand its influence on the morphology and pseudocapacitive properties of NiO, even though enhancement was observed in the electrochemical performance of NiO on nickel foams by combining the advantages of magnetic fields and the hydrothermal route.²⁸

Therefore, the aim of this work is to understand the influence of an external magnetic field on the structure and pseudocapacitive properties of NiO. Herein, the study reports the fabrication of NiO deposited on nickel foam through a magnetic-field-assisted hydrothermal reduction process with a post-annealing treatment. To optimize the electrochemical performance in an alkaline 3 M KOH electrolyte, we investigated the influence of a magnetic field (0–12.6 mT, applied by an electromagnetic coil) on the structure and morphology of NiO and the electrochemical behaviors of the electrodes.

Experimental

Materials

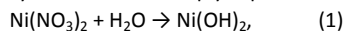
The main chemicals used in this work were Ni(NO₃)₂·6H₂O, HCl (37 wt.%) and KOH from Shanghai Sinopharm Chemical Reagent Company, China. Nickel foams were purchased from Jiangsu Kunshan Dessco Electronic Company. All the chemicals used in this work were of analytical grade without further purification.

Synthesis of Nanostructured NiO electrodes under magnetic fields

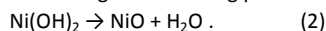
Nickel foams (1 × 2 cm², 3.9 m² g⁻¹) were carefully cleaned with a 5 M HCl solution for 30 minutes to remove the NiO layer from the surface and then washed repeatedly with acetone, ethanol, and deionized water for several times before use. In the present synthesis, 0.3 g nickel nitrate was dissolved in 20 ml deionized water under stirring, which resulted in a green colored solution. Then pretreated nickel foam substrates and the solution were transferred into a 25 ml Teflon-lined stainless steel autoclave. Afterwards, the sealed autoclaves were heated at 100 °C for 6 h in an oven for the hydrothermal process. An external magnetic field was applied around the stainless steel autoclave by an electromagnetic coil (Φ: 10 cm, coil turns: ~900), which was wound by enamelled copper wire (weight 1.5 kg, Φ: 0.8 mm). Fig. 1(a) exhibits a diagrammatic sketch of the experimental setup. When the current varies from 0 to 2.0 A controlled by the DC power supplier, the electromagnetic coil produced magnetic fields ranging from 0 to 12.6 mT in the region marked by the red circle in Fig. 1(a), measured by a GM55 Gaussmeter (Shanghai Golden-magnet Technology Co., Ltd). The relationship between the magnetic field strength and the current has been shown in Fig. 1(b). After being cooled to room temperature, the substrates covered with green deposits were picked out, washed with deionized water, and dried

at 80 °C for 12 h. Finally, the samples were annealed at 300 °C in air for 2 h with a ramping rate of 5 °C min⁻¹ to form NiO. Accordingly, the obtained electrodes were named as MF-NiO-*x*A (*x* means the current, *x*=0, 0.5, 1.0, 1.5 and 2.0). The average deposits of the resultant NiO loaded on the nickel foams weighed ~2.0 mg cm⁻².

The chemical reaction involved in the present hydrothermal synthesis can be simply expressed as follows:



and during the annealing process:



Materials characterization

The nickel foams and NiO electrodes were weighed by a high-precision electronic balance (Mettler Toledo AG245). The structure of the NiO electrodes was characterized by X-ray diffraction (XRD; D/max-rC with Cu K_α radiation) in the 2θ range of 20–90° with the scan rate of 8° min⁻¹. The microstructure and morphology were characterized by a field emission scanning electron microscope (FE-SEM; Quanta FEG-250) operated at 7 kV. High resolution transmission electron microscopy (HR-TEM) images were collected using a JEOL JEM-2100F electron microscope operating at an accelerating voltage of 200 kV.

Electrochemical characterization

The electrochemical tests were carried out in a three-electrode electrochemical cell with a 3M KOH aqueous solution as the electrolyte, using a CHI660D electrochemical workstation (Shanghai CH Instruments Co., Ltd.) at room temperature. The as-prepared NiO electrodes directly acted as the working electrode, while a platinum foil (1 × 4 cm²) was used as the counter electrode, and a saturated calomel electrode (SCE) was used as the reference electrode. The electrochemical performance of the NiO electrodes was tested by means of cyclic voltammetry (CV), galvanostatic charge-discharge (GC), and electrochemical impedance spectroscopy (EIS) measurements. Cycle life tests were conducted on a CT2001E battery program-controlled test system (Wuhan LAND electronics Co., Ltd.).

Results and discussion

Structural characterizations

Fig. 2 shows the x-ray diffraction spectra of MF-NiO-0A, MF-NiO-0.5A, MF-NiO-1.0A, MF-NiO-1.5A and MF-NiO-2.0A specimens. As shown in Fig. 2, except for the three strongest peaks from the substrate nickel, three well-defined diffraction peaks are observed at 37.0°, 42.9° and 62.4°, which can be indexed as (111), (200), and (220) crystal planes of a cubic NiO phase (JCPDS, No. 47-1049). These results suggest that all specimens are virtually of a single NiO phase, which is successfully grown upon the nickel foam surface. The XRD results show that the magnetic field has no significant effects on the phase of the NiO electrodes.

Figs. 3(a), (c) and (e) show representative FE-SEM images of surface morphology of MF-NiO-0A, MF-NiO-1.5A, and MF-NiO-2.0A, respectively. It can be easily seen in Fig. 3(a) that the NiO films exhibit a structure consisting of uniform hexagonal nanoplates. These nanoplates are approximately perpendicular to the substrate's surface, and several nanoplates may stack together to form larger ones with 500–700 nm in the hexagon side length and

~80 nm in thickness. In addition, due to the irregular arrangement of the NiO nanoplates, many gaps are formed at the surface of the film. Fig. 3(c) and (e) show that both MF-NiO-1.5A and MF-NiO-2.0A nanoplates become smaller in the hexagon side length and thicker, with less gaps at the surface of the film. We can estimate that the side length of the hexagonal nanoplates is about 400-600 nm, and the thickness is 200 nm. Figs. 3(b), (d) and (f) exhibit the cross sections of the MF-NiO-0A, MF-NiO-1.5A and MF-NiO-2.0A films on the nickel foam, showing that the patchy distribution of the section become more regular after applying the magnetic field. The thicknesses of the NiO layers are about 858.7 nm, 768.4 nm, and 1068 nm, respectively. These show that the NiO film as a low-dimensional magnetic system can become anisotropic under an anisotropic magnetic force, because the NiO nanoplates had nucleated and then were arranged and grew under the magnetic field.^{29, 30}

Fig. 4(a)-(e) show the HR-TEM images for the MF-NiO-0A, MF-NiO-1.5A and MF-NiO-2.0A samples, respectively. It can be seen that all the samples are of porous structures. It is worth noting that the lengths of hexagons' sides are about 300 nm, 200 nm, and 200 nm, respectively, for the MF-NiO-0A, MF-NiO-1.5A, and MF-NiO-2.0A (Fig. 4(a), (c) and (e)). Detailed structural information of the nanoplates can be obtained by analyzing the lattice fringes in the HR-TEM images. Fig. 4(b) shows clearly that the lattice spaces are 0.208 nm and 0.240 nm, which agree well with the interplanar distance of the (200) and (111) planes of NiO (JCPDS, No. 47-1049). The interplanar spacing remains almost unchanged, i.e., 0.243 nm of the (111) plane for MF-NiO-1.5A nanoplates (Fig. 4(d)).

Based on the discussions about the FE-SEM and HR-TEM images, we propose a formation mechanism as shown graphically in Fig. 5. During the hydrothermal reaction, Ni²⁺ combines with OH⁻ by electrostatic adsorption, and each Ni²⁺ ion is bound to six hydroxyl groups. The [Ni(OH)₆]⁴⁻ groups self-assemble to form the octahedrons of Ni(OH)₂. The octahedrons share their edges to form two-dimensional hexagonal nanoplates, which then stack upon one another to form a nanoplate.³¹ However, to make good adhesion with the nickel foam, the precursors of NiO grow into uniform irregular hexagonal structure instead of regular hexagons, as shown in FE-SEM and HR-TEM.³² During the annealing process, hydroxyl groups from adjacent layers combine and form water molecules, which escape from the lattice, leaving behind molecule-sized pores. By this process, the precursor Ni(OH)₂ successfully decomposes into NiO and form pores within the nanoplates. Such porosity would create more channels for electrolyte ions to transport through and to electrochemically access even more electroactive sites for pseudocapacitance reactions than a dense NiO film.^{31, 33}

As much effort has been devoted to the influence of a magnetic force on microstructures in deposition processes, some researchers concluded that a constant uniform magnetic field and a gradient magnetic field should result in different effects on the microstructures.^{34, 35} In Fig. 1(a), the length of the nickel foam (1 cm) is about 10% of the diameter of the electromagnetic coil (10 cm) and the variation of the magnetic field strength is about 0.1 mT in the red circle region from our measurement. Thus, we consider the magnetic field as homogeneous, and ignore any stray magnetic field of the stainless steel autoclave and nickel foam. During the hydrothermal reaction, the very thin nanoplates were

first deposited on the nickel foam, and then became thicker and larger. Finally, the single nanoplate tends to self-assemble to form spike-piece-structured Ni(OH)₂ to minimize the overall surface energy.³⁶ When the external magnetic field was applied, the magnetic dipoles of the Ni²⁺ ions are affected by the magnetic force, and the surface energy of NiO would be decreased under external magnetic field. However, the decline rate of energy with different faces of NiO was different.³⁷ As a result, the magnetic force may play an important role in the growth on (111) along the [111] of the NiO nanoplates, and promoting to form multilayer nanoplate array structure.^{33, 38} From the change in the size of the nanoplates of MF-NiO-0A and MF-NiO-1.5A, it may be the kinetics which was influenced by the magnetic field. The detailed FE-SEM and HR-TEM analyses indicated that the weak magnetic field had an influence on the surface energy of Ni(OH)₂, and therefore had a significant impact on surface and cross-sectional structures of the NiO films.

Electrochemical properties of NiO electrodes

Cyclic voltammetry (CV), galvanostatic charge-discharge measurements (GC), and electrochemical impedance spectroscopy (EIS) measurements have been employed to evaluate the electrochemical properties of the as-prepared electrodes (MF-NiO-xA, where x=0, 0.5, 1.0, 1.5 and 2.0) in 3 M KOH aqueous solution. Fig. 6(a) shows the CV curves of the five samples scanned in the potential range between 0 and 0.5 V (vs. SCE) at a scan rate of 5 mV s⁻¹. As some studies showed that the pretreated nickel foam had noticeable capacitance properties in KOH electrolytes, this could bring errors to the measured specific capacitance of the active electrode materials.³⁹ To solve this problem, we first measured the C-V curve of the blank nickel foam (i.e., without NiO) under identical conditions. It showed that there was no significant pseudocapacitance in the strong alkaline media, as the peak current was less than 2 mA cm⁻², such that the contribution of the nickel foam to the capacitance of the whole electrode was small and could be ignored in this study. The CV curve of the NiO film typically includes two strong peaks based on a redox mechanism. The oxidation peaks are at around 0.3 V and the reduction peaks are at 0.1-0.2 V. These peaks are due to the conversion between NiO and NiOOH. Corresponding to the redox process, it can be assigned to the processes of the exchange of OH⁻ and cations, as described by the following equation:^{21, 40, 41}



Obviously, the enclosed areas of the curves in Fig. 6(a) were in the sequence of MF-NiO-0A < MF-NiO-0.5A < MF-NiO-2.0A < MF-NiO-1.0A < MF-NiO-1.5A. The magnetic-field-assisted NiO show higher current densities of the redox couple peaks than those of the bare NiO film at the same scanning rate, indicating that the NiO synthesized under a magnetic field have higher electrochemical reaction activity, and more active materials participate in the oxidation/reduction reaction.

The charge/discharge curves of the NiO electrodes are presented in Fig. 6(b), which shows the supercapacitive performance tested in a potential window of 0 to 0.4 V at a current density of 0.5 A g⁻¹. From these charge/discharge curves, the specific capacitance is derived by the formula:

$$C = I\Delta t / m\Delta V \quad (4)$$

Where I is the current, Δt is the time for the discharge cycle, m is the mass of the active material on the electrode, and ΔV is the potential drop during charge or discharge. As shown in table 1, the evaluated specific capacitance values of the electrodes are 726.5, 815.3, 927.0, 932.1, and 881.4 $F g^{-1}$ for the MF-NiO- x A ($x=0, 0.5, 1.0, 1.5$ and 2.0) at $0.5 A g^{-1}$, respectively. The best achieved capacitance, i.e., 932.1 $F g^{-1}$ of the MF-NiO-1.5A, is reasonably high in comparison with those values previously reported for NiO-based electrodes, such as NiO nanosheets on nickel foam substrate (349 $F g^{-1}$ at $0.25 A g^{-1}$),²⁰ well-aligned NiO nanosheets (943.5 $F g^{-1}$ at $5 A g^{-1}$),²⁵ and NiO nanowires (670 $F g^{-1}$ at $1 A g^{-1}$).⁴² In those reports, researchers prepared NiO of various morphologies such as nanospheres, nanosheets and nanowires. The different morphologies and microstructures showed substantial differences in electrochemical performance due to dissimilarities in the electrode/electrolyte interface properties and ion transfer rates during the charge storage processes.^{21,43} In the present study, the magnetic field improves the morphology and electrochemical performance of the NiO electrodes that are competitive for supercapacitor applications. As shown in FE-SEM, the uniform film with tidy NiO nanoplates of MF-NiO-1.5A exhibit a unique interlayer architecture that facilitates the soaking of electrolytes into the electrode materials, greatly enhancing the intercalation of the electrolyte ions and ensuring sufficient Faradaic reactions, which would be beneficial to the electrochemical performance. Compared with MF-NiO-1.5A, the relatively thicker film of MF-NiO-2.0A may hinder the reactions between the electrolyte and the active material, resulting in a slight decline in the electrochemical performance.

Fig. 7(a) shows the CV curves of the MF-NiO-1.5A at different scan rates ranging from 10 to 50 $mV s^{-1}$. With the increase of the scan rates, the anodic peaks and cathodic peaks of two electrodes shift toward positive potential and negative potential, indicating the reversible redox reactions. Fig. 7(b) shows the charge-discharge curves of the MF-NiO-1.5A at different current densities. As shown in Table 2, the specific capacitance values of the MF-NiO-1.5A electrode measured from the discharge curves are 932.1, 835.0, 799.0, 771.0 and 748.0 $F g^{-1}$ at the current densities of 0.5, 1.0, 2.0, 3.0 and 4.0 $A g^{-1}$, respectively. The capacitance retention is about 80.2%, indicating that the MF-NiO-1.5A has a good rate capability in KOH electrolyte. The decrease of the capacitance with the increase of the discharge current density is probably caused by the relatively insufficient faradic redox reaction of the active materials under higher discharge current densities.

The long-term cycle stability of the MF-NiO-0A and MF-NiO-1.5A is evaluated and the specific capacitance with respect to charge-discharge cycle number (up to 1000 cycles) at $2 A g^{-1}$ is shown in Fig. 8. The specific capacitances of the MF-NiO-0A and MF-NiO-1.5A are 572.3 and 853.1 $F g^{-1}$ and the capacitance retention rates are 80.6% and 91.9% after 1000 cycles, respectively, indicating that the MF-NiO-1.5A exhibits better cycle stability than the MF-NiO-0A over the entire cycle numbers. The high retention rate of MF-NiO-1.5A indicates high stability and cycling performance of this electrode material. The mechanism of degradation is mainly associated with a self-discharge phenomenon accompanying oxygen evolution. The self-discharge phenomenon results in a partial dissolution of NiO and the oxygen evolutions in

competition with the NiO/NiOOH electrochemical process during cycling. The produced oxygen bubbles can accelerate the degradation process by striking the film.⁴⁴ The enhanced cycling stability can be attributed to the interspaces between the NiO nanoplates, which could buffer the oxygen bubbles' striking and effectively restrain the degradation of NiO.

Electrochemical impedance spectroscopy (EIS) measurements were carried out in a frequency range of 10^{-2} to 10^5 Hz, which is applied to determine the conductivity, charge-transfer properties, diffusion properties of an electrode. Nyquist plots of the MF-NiO-0A, MF-NiO-0.5A, MF-NiO-1.5A and MF-NiO-2.0A are shown in Fig. 9. It is noticed that the impedance behavior might be dominated by two major processes occurring in the high- and low-frequency regions, respectively.⁴⁴ According to Fig. 9, the value of R_s , a combinational resistance of electrolyte resistance, intrinsic resistance of substrate, and contact resistance at the active material/current collector interface, are 0.78, 0.74, 0.66, and 0.67 Ω for the MF-NiO- x A ($x=0, 0.5, 1.5$ and 2.0), demonstrated as the intercept at real part (Z') of Nyquist plots. The low-frequency range is related to ion diffusion between electrolyte and electrode. The inclined lines for MF-NiO-0.5A, MF-NiO-1.5A, and MF-NiO-2.0A electrodes lean more towards the imaginary axis than that of the MF-NiO-0A electrode, and this implies a higher ion-diffusion rate. The lower resistance and higher ion-diffusion rate for the NiO electrodes mean a faster charge-transfer process and better electrolyte accessibility, both of which should be attributed to the morphology change caused by the magnetic field.

Conclusion

In summary, we reported a simple, facile and cost-effective hydrothermal synthesis of MF-NiO- x A (x means the current intensity, $x=0, 0.5, 1.0, 1.5$ and 2.0) electrodes on the nickel foam in the present study. The magnetic field plays a positive role in controlling the growth of NiO nanoplates, resulting in a significant variation in the morphology and electrochemical performance of NiO electrodes. Among all the samples, the MF-NiO-1.5A electrode reaches an optimal specific capacitance of 932.1 $F g^{-1}$ at $0.5 A g^{-1}$ and shows a good capacitance retention rate of 91.9% at $2.0 A g^{-1}$ after 1000 cycles in 3 M KOH electrolyte. Therefore, the NiO electrodes synthesized with magnetic fields are suitable as electrode materials of supercapacitors.

Acknowledgement

The study is primarily supported by Shanghai Eastern-scholar program and Shanghai Pujiang Program, China. The authors thank the support from the Instrumental Analysis and Research Center of Shanghai University.

References

- Ramachandran, R., Felix, S., Saranya, M., Santhosh, C., Velmurugan, V., Ragupathy, B. P. C., Jeong, S. K. & Grace, A. N. (2013). Synthesis of Cobalt Sulfide-Graphene (CoS/G) Nanocomposites for Supercapacitor Applications. *IEEE Trans Nanotechnol.* 12, 985-990.
- Simon, P. & Gogotsi, Y. (2008). Materials for electrochemical capacitors. *Nat Mater.* 7, 845-854.
- Wang, C. D., Xu, J. L., Yuen, M. F., Zhang, J., Li, Y. Y., Chen, X. F. & Zhang, W. J. (2014). Hierarchical Composite Electrodes of Nickel Oxide Nanoflake 3D Graphene for High-Performance Pseudocapacitors. *Adv Funct Mater.* 24, 6372-6380.
- Rajendran, R., Shrestha, L. K., Kumar, R. M., Jayavel, R., Hill, J. P. & Ariga, K. (2015). Composite Nanoarchitectonics for Ternary Systems of Reduced Graphene Oxide/Carbon Nanotubes/Nickel Oxide with Enhanced Electrochemical Capacitor Performance. *J Inorg Organomet Polym Mater.* 25, 267-274.
- Su, Z. J., Yang, C., Xie, B. H., Lin, Z. Y., Zhang, Z. X., Liu, J. P., Li, B. H., Kang, F. Y. & Wong, C. P. (2014). Scalable fabrication of MnO₂ nanostructure deposited on free-standing Ni nanocone arrays for ultrathin, flexible, high-performance micro-supercapacitor. *Energy Environ Sci.* 7, 2652-2659.
- Wang, K. B., Zhang, Z. Y., Shi, X. B., Wang, H. J., Lu, Y. N. & Ma, X. Y. (2015). Temperature-dependent self-assembly of NiO/Co₃O₄ composites for supercapacitor electrodes with good cycling performance: from nanoparticles to nanorod arrays. *RSC Adv.* 5, 1943-1948.
- Hu, L. B., Chen, W., Xie, X., Liu, N. A., Yang, Y., Wu, H., Yao, Y., Pasta, M., Alshareef, H. N. & Cui, Y. (2011). Symmetrical MnO₂-Carbon Nanotube-Textile Nanostructures for Wearable Pseudocapacitors with High Mass Loading. *ACS Nano.* 5, 8904-8913.
- Zhang, J. T., Jiang, J. W., Li, H. L. & Zhao, X. S. (2011). A high-performance asymmetric supercapacitor fabricated with graphene-based electrodes. *Energy Environ Sci.* 4, 4009-4015.
- Jena, A., Munichandraiah, N. & Shivashankar, S. A. (2013). Carbonaceous nickel oxide nano-composites: As electrode materials in electrochemical capacitor applications. *J Power Sources.* 237, 156-166.
- Wang, G. X., Xu, H. F., Lu, L. & Zhao, H. (2015). One-step synthesis of mesoporous MnO₂/carbon sphere composites for asymmetric electrochemical capacitors. *J Mater Chem A.* 3, 1127-1132.
- Chuang, C. M., Huang, C. W., Teng, H. S. & Ting, J. M. (2012). Hydrothermally synthesized RuO₂/Carbon nanofibers composites for use in high-rate supercapacitor electrodes. *Compos Sci Technol.* 72, 1524-1529.
- Wang, Y. G., Wang, Z. D. & Xia, Y. Y. (2005). An asymmetric supercapacitor using RuO₂/TiO₂ nanotube composite and activated carbon electrodes. *Electrochim Acta.* 50, 5641-5646.
- Kim, E. K., Shrestha, N. K., Lee, W., Cai, G. & Han, S. H. (2015). Influence of water-soluble conjugated/non-conjugated polyelectrolytes on electrodeposition of nanostructured MnO₂ film for supercapacitors. *Mater Chem Phys.* 155, 211-216.
- Reddy, R. N. & Reddy, R. G. (2003). Sol-gel MnO₂ as an electrode material for electrochemical capacitors. *J Power Sources.* 124, 330-337.
- Zhu, T., Zheng, S. J., Chen, Y. G., Luo, J., Guo, H. B. & Chen, Y. E. (2014). Improvement of hydrothermally synthesized MnO₂ electrodes on Ni foams via facile annealing for supercapacitor applications. *J Mater Sci.* 49, 6118-6126.
- Zhang, F. B., Zhou, Y. K. & Li, H. L. (2004). Nanocrystalline NiO as an electrode material for electrochemical capacitor. *Mater Chem Phys.* 83, 260-264.
- Yang, J., Lan, T. B., Liu, J. D., Song, Y. F. & Wei, M. D. (2013). Supercapacitor electrode of hollow spherical V₂O₅ with a high pseudocapacitance in aqueous solution. *Electrochim Acta.* 105, 489-495.
- Xia, X. H., Tu, J. P., Zhang, Y. Q., Mai, Y. J., Wang, X. L., Gu, C. D. & Zhao, X. B. (2012). Freestanding Co₃O₄ nanowire array for high performance supercapacitors. *RSC Adv.* 2, 1835-1841.
- An, L., Xu, K. B., Li, W. Y., Liu, Q., Li, B., Zou, R. J., Chen, Z. G. & Hu, J. Q. (2014). Exceptional pseudocapacitive properties of hierarchical NiO ultrafine nanowires grown on mesoporous NiO nanosheets. *J Mater Chem A.* 2, 12799-12804.
- Lv, S., Wang, C. G. & Xing, S. G. (2014). Hexamethylenetetramine-induced synthesis of hierarchical NiO nanostructures on nickel foam and their electrochemical properties. *J Alloy Compd.* 603, 190-196.
- Wang, H. W., Yi, H., Chen, X. & Wang, X. F. (2013). Facile synthesis of a nano-structured nickel oxide electrode with outstanding pseudocapacitive properties. *Electrochim Acta.* 105, 353-361.
- Shin, D. H., Lee, J. S., Jun, J. & Jang, J. (2014). Fabrication of amorphous carbon-coated NiO nanofibers for electrochemical capacitor applications. *J Mater Chem A.* 2, 3364-3371.
- Xia, X. H., Tu, J. P., Zhang, Y. Q., Wang, X. L., Gu, C. D., Zhao, X. B. & Fan, H. J. (2012). High-Quality Metal Oxide Core/Shell Nanowire Arrays on Conductive Substrates for Electrochemical Energy Storage. *ACS Nano.* 6, 5531-5538.
- Yin, J. L. & Park, J. Y. (2014). A nickel foam supported copper core/nickel oxide shell composite for supercapacitor applications. *Micropor Mesopor Mat.* 200, 61-67.
- Yan, H. L., Zhang, D. Y., Xu, J. Y., Lu, Y., Liu, Y. X., Qiu, K. W., Zhang, Y. H. & Luo, Y. S. (2014). Solution growth of NiO nanosheets supported on Ni foam as high-performance electrodes for supercapacitors. *Nanoscale Res Lett.* 9, 424.
- Yang, L., Qian, L., Tian, X. Q., Li, J., Dai, J. Y., Guo, Y. & Xiao, D. (2014). Hierarchically Porous Nickel Oxide Nanosheets Grown on Nickel Foam Prepared by One-Step In Situ Anodization for High-Performance Supercapacitors. *Chem-Asian J.* 9, 1579-1585.
- Wang, J., Wei, L. M., Zhang, L. Y., Jiang, C. H., Kong, E. S. W. & Zhang, Y. F. (2012). Preparation of high aspect ratio nickel oxide nanowires and their gas sensing devices with fast response and high sensitivity. *J Mater Chem* 22, 8327-8335.
- Wang, G. X., Cai, J., Xu, H. F., Lu, L. & Zhao, H. (2014). Enhanced capacitance of a NiO electrode prepared in the magnetic field. *J Appl Electrochem.* 44, 391-398.
- Das, S., Majumdar, S. & Giri, S. (2010). Magnetic Field, Temperature, and Time Controlled Manipulation of Switching Mechanism in NiO Film: Evidence of Large Magnetoconductance. *J. Phys. Chem. C.* 114, 6671-6675.
- Zhang, M., Deng, J., Zhang, M. H. & Li, W. (2009). Shape-Controlled Synthesis of Nickel Wires Using an External Magnetic Field. *Chin. J. Catal.* 30, 447-452.
- Zhu, Z. H., Ping, J., Huang, X. P., Hu, J. G., Chen, Q. Y., Ji, X. B. & Banks, C. E. (2012). Hexagonal nickel oxide nanoplate-based electrochemical supercapacitor. *J Mater Sci.* 47, 503-507.
- Min, S. D., Zhao, C. J., Zhang, Z. M., Chen, G. R., Qian, X. Z. & Guo, Z. P. (2015). Synthesis of Ni(OH)₂/RGO pseudocomposite on nickel foam for supercapacitors with superior performance. *J Mater Chem A.* 3, 3641-3650.
- Lin, L. Y., Liu, T. M., Miao, B. & Zeng, W. (2013). Hydrothermal fabrication of uniform hexagonal NiO nanosheets: Structure, growth and response. *Mater Lett.* 102, 43-46.
- Gorobets, O. Y., Gorobets, V. Y., Derecha, D. O. & Brukva, O. M. (2008). Nickel electrodeposition under influence of constant

homogeneous and high-gradient magnetic field. *J Phys Chem C*. 112, 3373-3375.

35. Gorobets, O. Y., Gorobets, Y. I., Rospotniuk, V. P., Kyba, A. A. & Legenkiy, Y. A. (2015). Liquid-liquid phase separation occurring under the influence of inhomogeneous magnetic field in the process of the metal deposition and etching of the magnetized ferromagnetic ball. *J Solid State Electrochem*. DOI 10.1007/s10008-10015-12904-x.

36. Wu, L. C., Chen, Y. J., Mao, M. L., Li, Q. H. & Zhang, M. (2014). Facile Synthesis of Spike-Piece-Structured Ni(OH)(2) Interlayer Nanoplates on Nickel Foam as Advanced Pseudocapacitive Materials for Energy Storage. *Acs Applied Materials & Interfaces*. 6, 5168-5174.

37. Wang, M. S. & Chen, Q. W. (2010). Experimental and Theoretical Investigations on the Magnetic-Field-Induced Variation of Surface Energy of Co3O4 Crystal Faces. *Chem.-Eur. J*. 16, 12088-12090.

38. Abramson, S., Dupuis, V., Neveu, S., Beaunier, P. & Montero, D. (2014). Preparation of Highly Anisotropic Cobalt Ferrite/Silica Microellipsoids Using an External Magnetic Field. *Langmuir*. 30, 9190-9200.

39. Xing, W., Qiao, S. Z., Wu, X. Z., Gao, X. L., Zhou, J., Zhuo, S. P., Hartono, S. B. & Hulicova-Jurcakova, D. (2011). Exaggerated capacitance using electrochemically active nickel foam as current collector in electrochemical measurement. *J Power Sources*. 196, 4123-4127.

40. Hu, C. C., Chang, K. H. & Hsu, T. Y. (2008). The synergistic influences of OH(-) concentration and electrolyte conductivity on the redox behavior of Ni(OH)(2)/NiOOH. *J Electrochem Soc*. 155, F196-F200.

41. Xia, X. H., Tu, J. P., Wang, X. L., Gu, C. D. & Zhao, X. B. (2011). Hierarchically porous NiO film grown by chemical bath deposition via a colloidal crystal template as an electrochemical pseudocapacitor material. *J Mater Chem*. 21, 671-679.

42. Vidhyadharan, B., Zain, N. K. M., Misnon, II, Abd Aziz, R., Ismail, J., Yusoff, M. M. & Jose, R. (2014). High performance supercapacitor electrodes from electrospun nickel oxide nanowires. *J Alloy Compd*. 610, 143-150.

43. Dalavi, D. S., Suryavanshi, M. J., Mali, S. S., Patil, D. S. & Patil, P. S. (2012). Efficient maximization of coloration by modification in morphology of electrodeposited NiO thin films prepared with different surfactants. *J Solid State Electrochem*. 16, 253-263.

44. Huang, M. L., Gu, C. D., Ge, X., Wang, X. L. & Tu, J. P. (2014). NiO nanoflakes grown on porous graphene frameworks as advanced electrochemical pseudocapacitor materials. *J Power Sources*. 259, 98-105.

Table 1 The specific capacitance values of the five electrodes (at a current density of 0.5 A g^{-1})

magnetic field strength (applied current)	0 mT (0 A)	3.2 mT (0.5 A)	6.3 mT (1.0 A)	9.5 mT (1.5 A)	12.6 mT (2.0 A)
$C (\text{F g}^{-1})$	726.5	815.3	927.0	932.1	881.4

Table 2 The specific capacitance values of MF-NiO-1.5A at different current densities

	0.5 A g^{-1}	1.0 A g^{-1}	2.0 A g^{-1}	3.0 A g^{-1}	4.0 A g^{-1}
$C (\text{F g}^{-1})$	932.1	835.0	799.0	771.0	748.0

Figure captions:

Fig. 1 (a) The diagrammatic sketch of the experimental setup, (b) Magnetic field strength of the electromagnetic coil as a function of the current

Fig. 2 XRD patterns of the NiO samples

Fig. 3 FE-SEM images of (a, b) MF-NiO-0A, (c,d) MF-NiO-1.5A, and (e,f) MF-NiO-2.0A

Fig. 4 HR-TEM images of (a, b) MF-NiO-0A, (c, d) MF-NiO-1.5A, and (e) MF-NiO-2.0A

Fig. 5 The proposed formation mechanism of the nano-NiO

Fig. 6 (a) Cyclic voltammetric plots of the five NiO electrodes at 5 mV s^{-1} , (b) Charge/discharge curves of the five NiO electrodes at 0.5 A g^{-1}

Fig. 7 (a) CV curves of MF-NiO-1.5A at different scan rates, (b) Charge/discharge curves of MF-NiO-1.5A at different current densities

Fig. 8 Cycle life of MF-NiO-0A and MF-NiO-1.5A tested at 2 A g^{-1}

Fig. 9 A.C. impedance plots of the MF-NiO-xA (x=0, 0.5, 1.5 and 2.0) electrodes

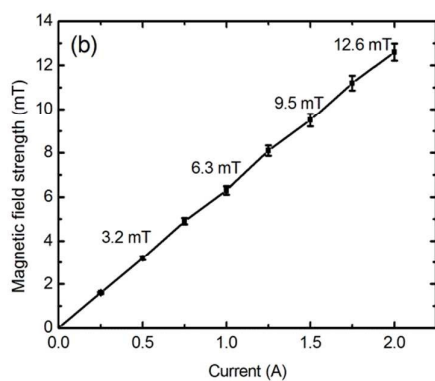
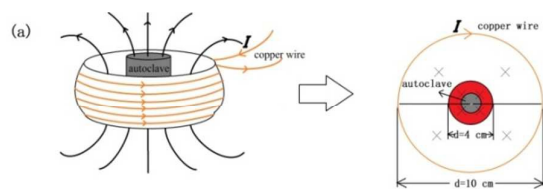


Fig. 1

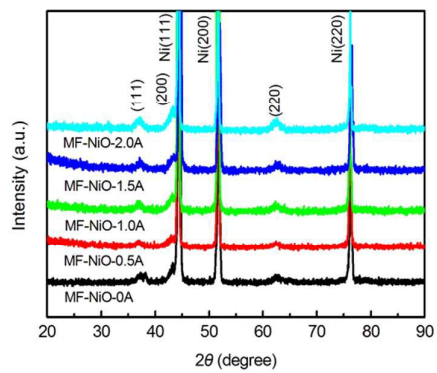


Fig. 2

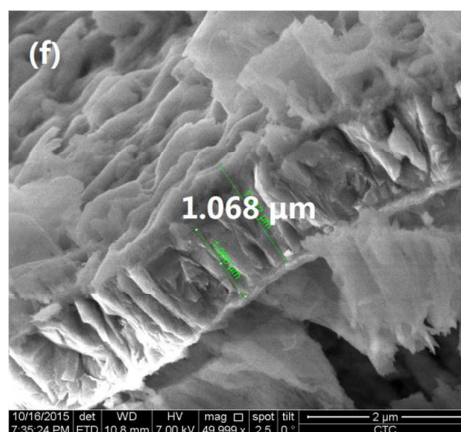
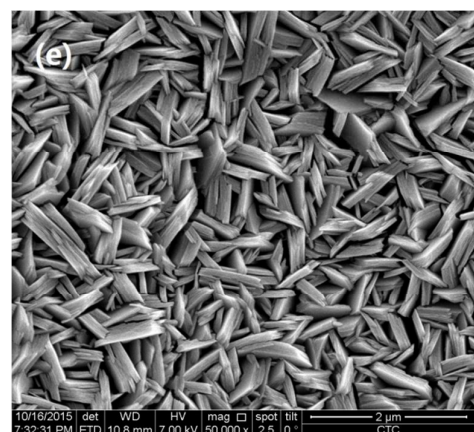
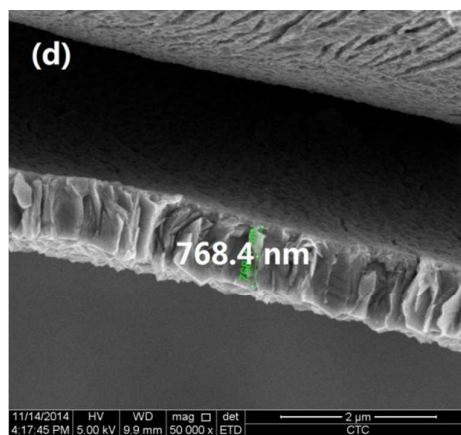
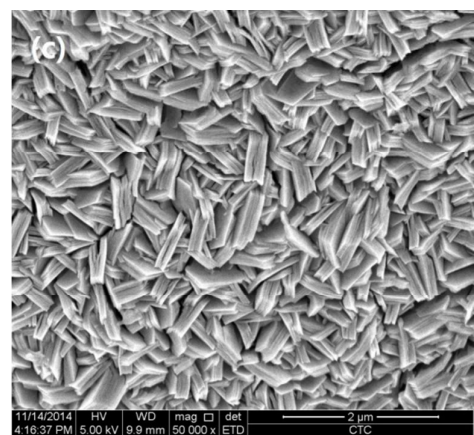
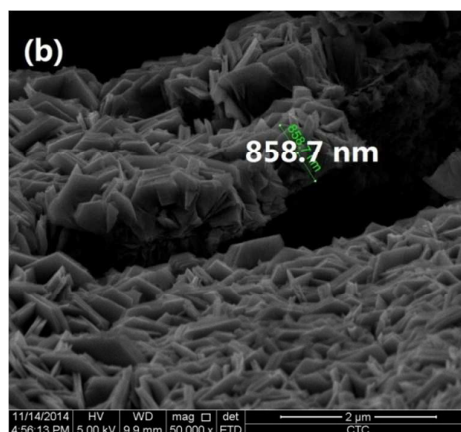
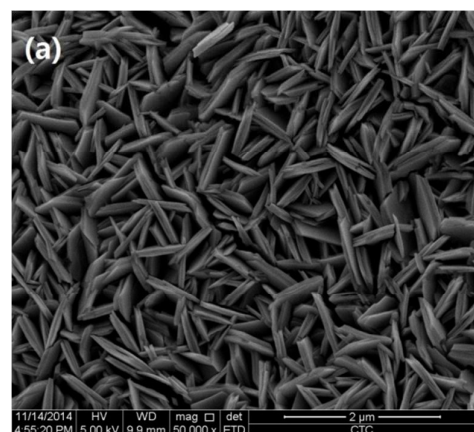


Fig. 3

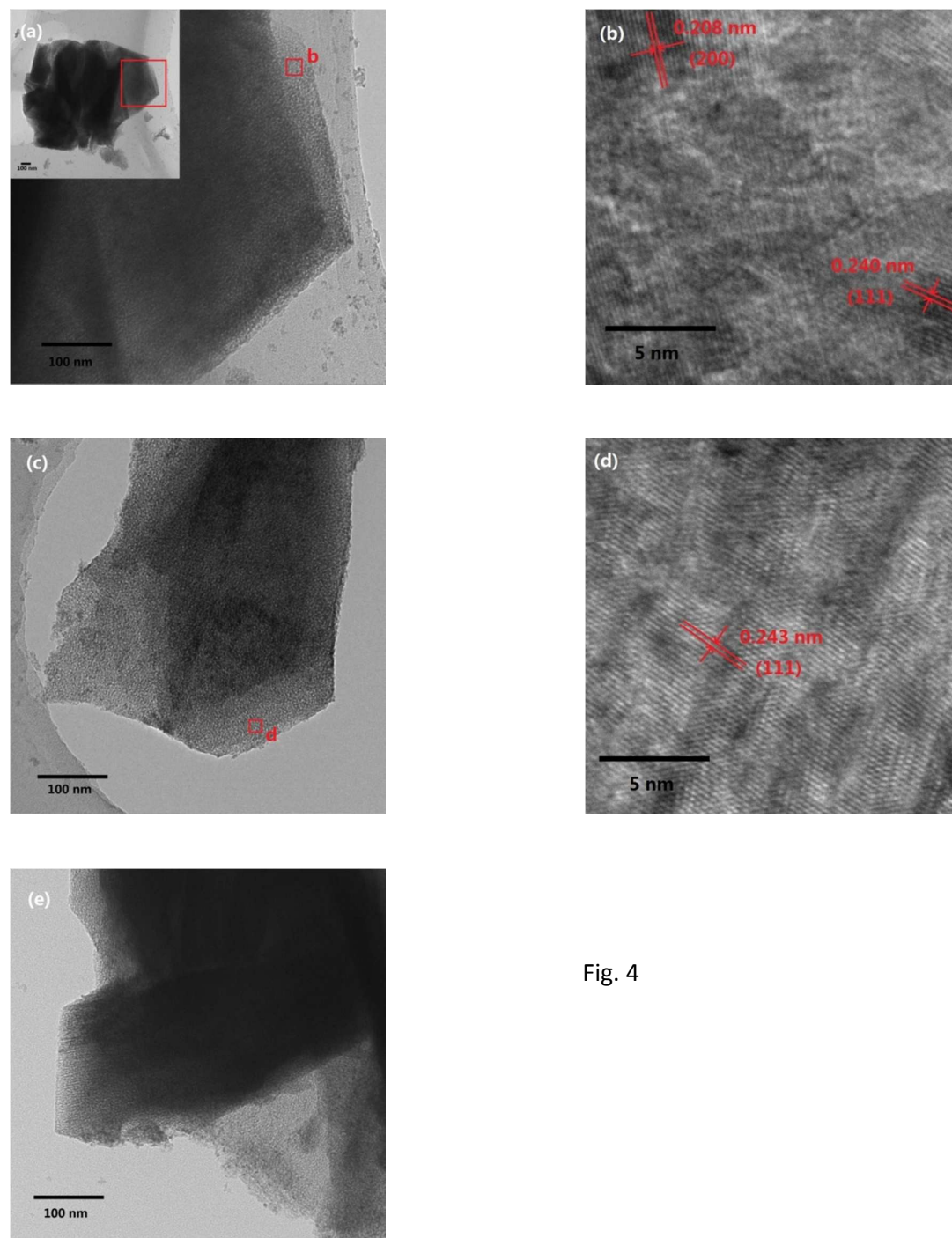


Fig. 4

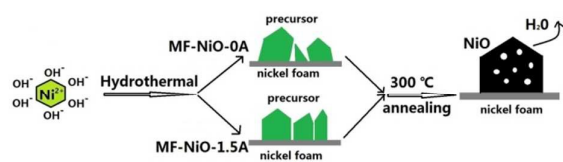


Fig. 5

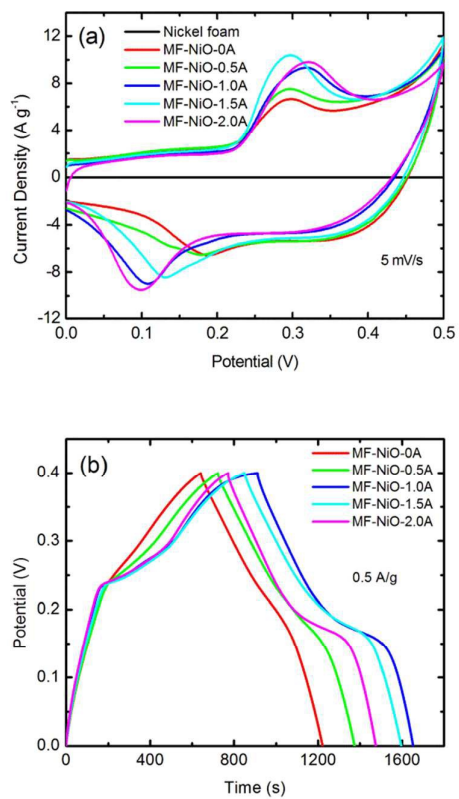


Fig. 6

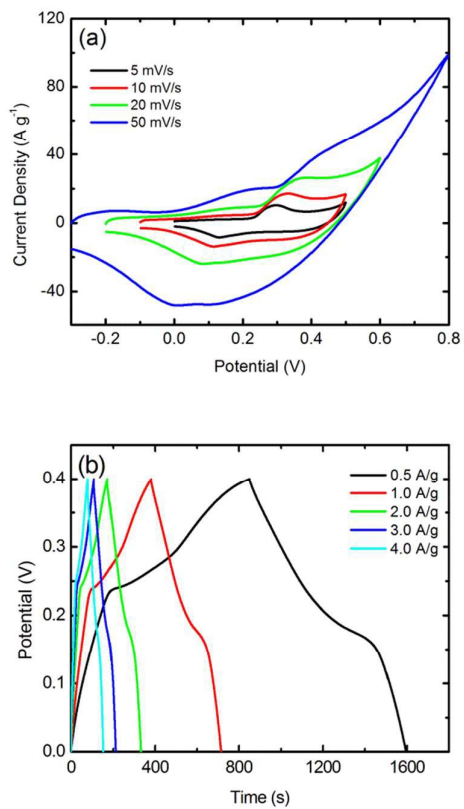


Fig. 7

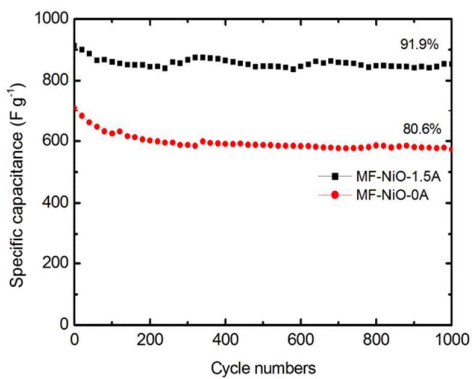


Fig. 8

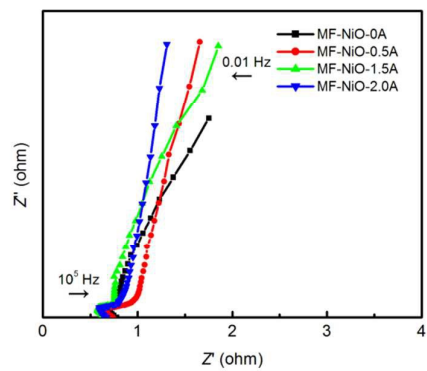


Fig. 9